

Strong magnetic frustration in $\text{Y}_3\text{Cu}_9(\text{OH})_{19}\text{Cl}_8$: a distorted kagome antiferromagnet

Pascal Puphal,¹ Michael Bolte,² Denis Sheptyakov,³ Andrej Pustogow,⁴
Kristin Kliemt,¹ Martin Dressel,⁴ Michael Baenitz,⁵ and Cornelius Krellner¹

¹*Physikalisches Institut, Goethe-University Frankfurt, 60438 Frankfurt am Main, Germany*

²*Institut für Organische Chemie der Universität Frankfurt, 60439 Frankfurt am Main, Germany*

³*Laboratory for Neutron Scattering and Imaging,*

Paul Scherrer Institute, 5232 Villigen, Switzerland

⁴*1. Physikalisches Institut, Stuttgart University, 70569 Stuttgart, Germany*

⁵*Max Planck Institute for Chemical Physics of Solids, D-01187 Dresden, Germany*

We present the crystal structure and magnetic properties of $\text{Y}_3\text{Cu}_9(\text{OH})_{19}\text{Cl}_8$, a stoichiometric frustrated quantum spin system with slightly distorted kagome layers. Single crystals of $\text{Y}_3\text{Cu}_9(\text{OH})_{19}\text{Cl}_8$ were grown under hydrothermal conditions. The structure was determined from single crystal X-ray diffraction and confirmed by neutron powder diffraction. The observed structure reveals two different Cu-positions leading to a slightly distorted kagome layer in contrast to the closely related $\text{YCu}_3(\text{OH})_6\text{Cl}_3$. Curie-Weiss behavior at high-temperatures with a Weiss-temperature θ_W of the order of -100 K, shows a large dominant antiferromagnetic coupling within the kagome planes. Specific-heat and magnetization measurements on single crystals reveal an antiferromagnetic transition at $T_N = 2.2$ K indicating a pronounced frustration parameter of $\theta_W/T_N \approx 50$. Optical transmission experiments on powder samples and single crystals confirm the structural findings. Specific-heat measurements on $\text{YCu}_3(\text{OH})_6\text{Cl}_3$ down to 0.4 K confirm the proposed quantum spin-liquid state of that system. Therefore, the two Y-Cu-OH-Cl compounds present a unique setting to investigate closely related structures with a spin-liquid state and a strongly frustrated AFM ordered state, by slightly releasing the frustration in a kagome lattice.

I. INTRODUCTION

Quantum spin systems with Cu^{2+} ions are suitable materials to study quantum many-body effects under variable conditions. Prominent examples are low-dimensional materials with strong magnetic frustrations. In these systems, a quantum spin-liquid state can be realized at low temperatures which is a highly correlated state that has no static magnetic order, despite sizeable magnetic interactions [1]. Compounds with decoupled antiferromagnetic kagome layers are prototypical systems to search for an experimental realization of the quantum spin-liquid state and Herbertsmithite, $\text{ZnCu}_3(\text{OH})_6\text{Cl}_2$, has become one of the most prominent materials in recent years [2–5].

The dominant magnetic interaction in Herbertsmithite is caused by Cu-O-Cu antiferromagnetic superexchange with an exchange energy of $J \sim 17$ meV, but no magnetic long-range order has been observed down to $T = 50$ mK [5]. Therefore, the spin-liquid ground-state of this material could be investigated in great detail (see e.g. a recent review in [6]). One structural drawback of Herbertsmithite is the intrinsic Zn-Cu-antisite disorder, which makes it challenging to achieve a structurally perfect $\text{ZnCu}_3(\text{OH})_6\text{Cl}_2$ crystal. Furthermore, the amount of antisite disorder is difficult to quantify with X-ray scattering techniques [6, 7]. Several structural variants including polymorphism with varying intersite Cu-M mixing are common features of Cu-based kagome compounds such as: Herbertsmithite - Kapellasite [5, 8], Mg-Herbertsmithite - Haydeaitite [9], Volborthite - Vesigniet [10, 11], Francisite [12] and Centenni-

alite [13]. From this point of view, novel kagome systems with highly ordered crystal structures are essential to uncover the intrinsic properties of the kagome antiferromagnet. In addition, the frontier of Herbertsmithite is chemical doping [6] since Mazin et al. have proposed that a correlated Dirac metal can be found in electron-doped Herbertsmithite which might be realized by replacing Zn by a trivalent ion [14].

Recently, W. Sun et al. reported on a non-hydrothermal synthesis of $\text{YCu}_3(\text{OH})_6\text{Cl}_3$ with LiOH and LiCl as pH regulating additives [15], enclosed in an autoclave to trap the crystal water. The reported structure is $P\bar{3}m1$ with one crystallographic copper position revealing a perfect two-dimensional kagome lattice. The determined crystal structure is more reminiscent to what was found in Kapellasite, a structural polymorph of Herbertsmithite [16]. They also show with Rietveld refinement of X-ray diffraction (XRD) data and nuclear magnetic resonance (NMR) that there is no significant Y - Cu exchange. In magnetic measurements on polycrystalline samples with small amounts of impurity phases Sun et al. see no magnetic order down to 2 K. The authors report that the absence of free water in the starting mixtures has been proven to be a key factor in the formation (and preservation) of this structural variant.

Here, we report on a different synthesis procedure in the Y-Cu-OH-Cl system and we obtain single crystals of $\text{Y}_3\text{Cu}_9(\text{OH})_{19}\text{Cl}_8$ from the hydrothermal method. For $\text{Y}_3\text{Cu}_9(\text{OH})_{19}\text{Cl}_8$, we find $R\bar{3}$ as the resulting structure with two distinct copper positions and two fully occupied yttrium positions. As a consequence $\text{Y}_3\text{Cu}_9(\text{OH})_{19}\text{Cl}_8$ presents the stoichiometric case of a slightly distorted

kagome system, leading to the stabilization of magnetic order at $T_N = 2.2$ K but a large portion of the spin degrees of freedom remain fluctuating. Therefore, $Y_3Cu_9(OH)_{19}Cl_8$ and $YCu_3(OH)_6Cl_3$ are ideal systems to investigate the change of a spin-liquid state to a strongly frustrated AFM ordered state, by slightly releasing the frustration in a kagome lattice.

II. EXPERIMENTAL

A. Synthesis

Single crystals of $Y_3Cu_9(OH)_{19}Cl_8$ were prepared in a hydrothermal Parr 4625 autoclave with a 575 ml filling capacity operated by a Parr 4842 power supply including a 982 Watlow controller. The crystals have blue to green colour and a hexagonal shape, typical sizes are up to $1 \times 1 \times 0.25$ mm³. For the crystallization, we placed duran glass ampoules filled with the solution in the autoclave and filled it with distilled water to ensure the same pressure as in the ampoules. The ampoules were loaded with 0.59 g Y_2O_3 , 0.82 g CuO, 0.89 g $CuCl_2 \cdot 2(H_2O)$ and 10 ml distilled water and then sealed at air. The autoclave was heated up to 270°C in four hours and subsequently cooled down to 260°C with 0.05 K/h, followed by a fast cooling to room temperature. Afterwards, the ampoules were opened and the content was filtered with distilled water. Unlike in the synthesis of the similar compounds (Herbertsmithite, $MgCu_3(OH)_6Cl_2$ Mg-Herbertsmithite [17], and $CdCu_3(OH)_6Cl_2$ [18]) there is no need to use excess Y in the growth, since the Y_2O_3 can easily be solved in chloridic solutions [19]. Attempts with an excess of YCl_3 in the solution in fact lead to a formation of $Y(OH)_3$. In addition, only the $x = 1$ stoichiometry of $Y_xCu_{4-x}(OH)_{6.33}Cl_{2.77}$ forms and we have not observed any phase with a x -value below 1, in contrast to the other compounds of this family.

Furthermore to compare the magnetic ground state of the two structural variants, we have reproduced the synthesis of polycrystalline $YCu_3(OH)_6Cl_3$ with the flux method from Ref. [15], where $Y(NO_3)_3 \cdot 6H_2O$ melts at 50°C, starting to form complexes [20]. We analysed the obtained powder with laser ablation - inductively coupled plasma - mass spectrometry (LA-ICP-MS). We found only a few ppm of Lithium and could therefore exclude lithium incorporation in $YCu_3(OH)_6Cl_3$.

B. Characterization

For the single crystal structure determination the data were collected at 173 K on a STOE IPDS II two-circle diffractometer with a Genix Microfocus tube with mirror optics using $Mo K_\alpha$ radiation ($\lambda = 0.71073$ Å). The data

were scaled using the frame scaling procedure in the X-AREA program system [21]. The structure was solved by direct methods using the program SHELXS [22] and refined against F^2 with full-matrix least-squares techniques using the program SHELXL-97 [22]. The H atoms bonded to O2, O3, and O4 were found in a difference map and were isotropically refined with the O-H distance restrained to 0.84(1) Å, whereas the H1 atom bonded to O1 was geometrically positioned and refined using a riding model. The crystal was twinned about $(-1 \ 0 \ 0/1 \ 1 \ 0/0 \ 0 \ -1)$ with a fractional contribution of 0.601(4) for the major domain. The space group $R\bar{3}$ was chosen, because the structure proved to be centrosymmetric (thus $R3$ could be excluded) and no hints for any mirror planes were detected (excluding space groups $R3m$ and $R\bar{3}m$). We measured neutron powder diffraction at the high-resolution powder neutron diffractometer HRPT [23], at the Paul Scherrer Institute in Villigen. An amount of ~ 1 g of $Y_3Cu_9(OH)_{19}Cl_8$ was enclosed into a vanadium can with an inner diameter of 6 mm and the measurement was carried out at room temperature with a wavelength of $\lambda = 1.494$ Å. The Rietveld refinement, of the neutron data, accomplishing the crystal structure was done using the fullprof suite [24]. Low-temperature diffraction data were collected with a Siemens D-500 diffractometer with $Cu K_\alpha$ radiation ($\lambda = 1.5406$ Å), here, the sample was placed on a Cu-sample holder in a Lakeshore M-22 closed cycle refrigerator.

For the optical characterization a Bruker Fourier-transform infrared spectrometer and a Woollam spectroscopic ellipsometer have been utilized. Optical transmission experiments in the mid-infrared range were performed with KBr powder pellets whereas thin flakes were used in the visible/UV range. The discussed features were also observed in single-crystalline samples of different thickness ($d = 15 - 70$ μm) proving them as bulk properties.

The specific-heat data and magnetic measurements were collected with the standard options of a Physical Property Measurement System from Quantum Design in a temperature range of 0.4 to 300 K.

III. RESULTS AND DISCUSSION

A. Crystal structure

TABLE I. Crystal structure parameters of $Y_3Cu_9(OH)_{19}Cl_8$ refined from X-ray single crystal diffraction data measured at 173 K. Space group $R\bar{3}$ (# 148). The unit cell parameters are $a = b = 11.5350(8)$ Å and $c = 17.2148(12)$ Å. All positions are fully occupied except H1, which has an occupancy of 1/6.

	Wyck.	x/a	y/b	z/c	U [Å ²]
Cu1	18f	0.66311(6)	0.82526(6)	0.50349(3)	0.00721(19)
Cu2	9d	0.5	1	0.5	0.0072(2)
Y1	6c	0.3333	0.6667	0.53850(4)	0.0075(2)
Y2	3b	1	1	0.5	0.0092(3)
Cl1	18f	0.66466(12)	1.00242(12)	0.61719(6)	0.0132(3)
Cl2	6c	1	1	0.33854(11)	0.0121(4)
O1	3a	0.3333	0.6667	0.6667	0.042(3)
H1	18f	0.404	0.7382	0.6561	0.063
O2	18f	0.8113(4)	0.8026(4)	0.54394(18)	0.0079(7)
H2	18f	0.813(6)	0.801(7)	0.5927(7)	0.012
O3	18f	0.5308(4)	0.6623(5)	0.55719(18)	0.0086(6)
H3	18f	0.555(6)	0.654(7)	0.6018(15)	0.013
O4	18f	0.5089(4)	0.8403(4)	0.46536(18)	0.0070(6)
H4	18f	0.492(6)	0.818(6)	0.4185(11)	0.011

The crystal structure of $Y_3Cu_9(OH)_{19}Cl_8$ is different from the theoretically proposed structure for electron-doped Herbertsmithite [14] as well as the structure reported by [15]. The additional electron from yttrium is bound with additional Cl^- / OH^- anions, so electron doping of Herbertsmithite was not successful in this structure. In agreement with Ref. [25], the Y-atoms are not incorporated into the interlayer site but in the kagome layer. Thus, $Y_3Cu_9(OH)_{19}Cl_8$ consists of repeating kagome layers. The distances between the Cu atoms are 3.2498 Å/3.3683 Å/3.3762 Å within the layer and 5.8607 Å/ 5.6788Å between the layers. In comparison, Herbertsmithite has Cu distances of 3.416 Å and 5.087 Å [7]. In Figure 1, the obtained crystal structure of $Y_3Cu_9(OH)_{19}Cl_8$ is shown. A comparison of the two similar structures can be made from Figure 1 b) and c). In contrast to $Y_3Cu_9(OH)_{19}Cl_8$, the $P\bar{3}m1$ structure has a partial disorder, for the two inequivalent Y positions, displayed as white parts of the sphere. The full occupancy of these two crystallographic Y positions in $Y_3Cu_9(OH)_{19}Cl_8$ causes the Cu-atoms to be slightly misaligned from a perfect plane. W. Sun et al. observed an increasing occupation of these disordered yttrium-atoms with decreasing temperature showing a tendency to the $R\bar{3}$ structure when lowering the temperature[15].

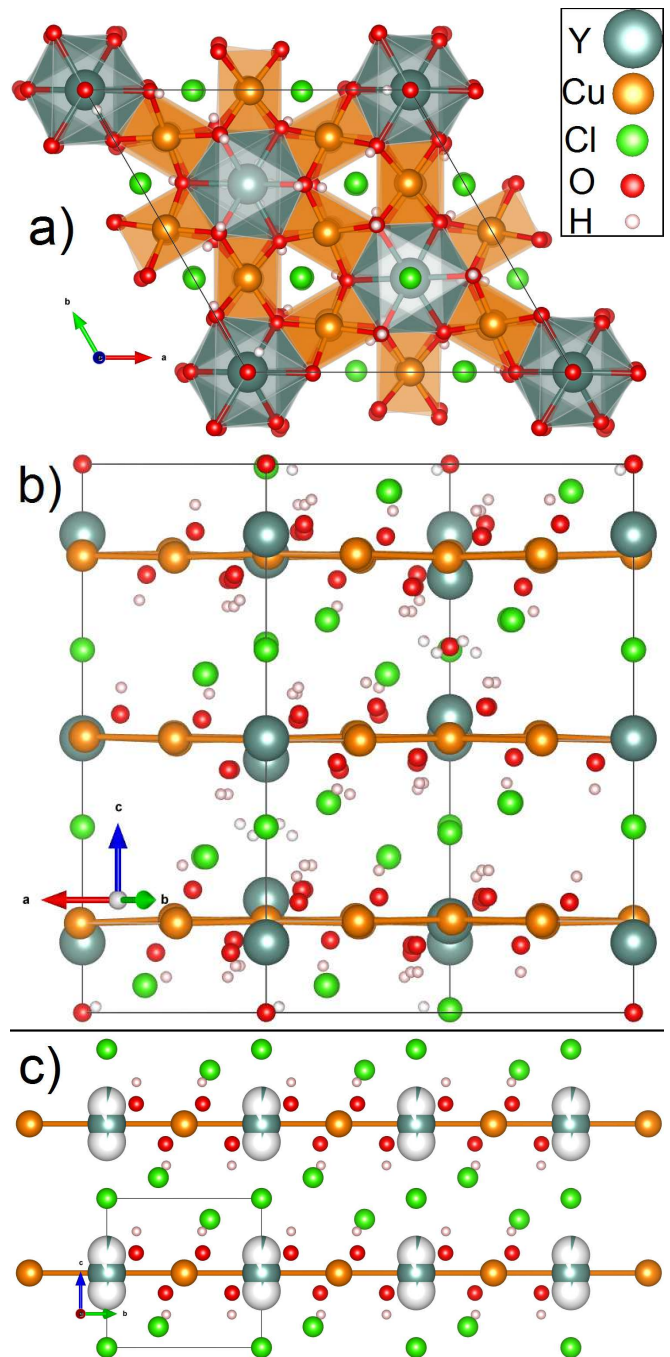


FIG. 1. Structure model of $Y_3Cu_9(OH)_{19}Cl_8$ (a,b) in comparison to $YCu_3(OH)_6Cl_3$ (c). a) Top view of the kagome layer in $Y_3Cu_9(OH)_{19}Cl_8$ crystallizing in the $R\bar{3}$ structure. b) Side view of the kagome layer in $Y_3Cu_9(OH)_{19}Cl_8$ stacked along the c -direction, where the slight buckling of the Cu-atoms due to two crystallographic positions is apparent. c) Side view of the kagome layer in $YCu_3(OH)_6Cl_3$ with the $P\bar{3}m1$ structure type [15] with a partially filled second position of Y.

A refinement plot based on the neutron powder diffraction data, at room temperature taken on 1 g of $Y_3Cu_9(OH)_{19}Cl_8$ is shown in Figure 2. The structure concept was obtained by the above described sin-

gle crystal X-ray data and the refinement of the neutron data confirmed that structure solution. A small amount of unreacted CuO and $\text{Cu}_2(\text{OH})_3\text{Cl}$ was observed in the large powder sample which formed due to the off-stoichiometric synthesis conditions. The unaccounted reflex part at 37° can also be accounted to some impurity phase.

It should be noted, that neutron scattering lengths of Y and Cu are in fact very close to each other: 7.75 and 7.718 fm, which makes them practically indistinguishable in neutron refinements. We therefore concluded the stoichiometric ordering without sizeable Y-Cu site exchange from the single-crystal X-ray refinement. There, the scattering cross sections for Y ($Z = 39$) and Cu ($Z = 29$) are sufficiently different.

TABLE II. Crystal structure parameters of $\text{Y}_3\text{Cu}_9(\text{OH})_{19}\text{Cl}_8$ refined from neutron diffraction data measured at 295 K. Space group $R\bar{3}$ (# 148). The unit cell parameters are $a = b = 11.5528(3)$ Å and $c = 17.2216(5)$ Å. All positions are fully occupied except H1, which has an occupancy of 1/6.

	Wyck.	x/a	y/b	z/c	U [Å ²]
Cu1	18f	0.6662(6)	0.8286(7)	0.5036(3)	0.0121(4)
Cu2	9d	0.5	1	0.5	0.0121(4)
Y1	6c	0.3333	0.6667	0.5393(3)	0.0074(9)
Y2	3b	1	1	0.5	0.0074(9)
Cl1	18f	0.6636(7)	0.9959(7)	0.61849(17)	0.0220(5)
Cl2	6c	1	1	0.3379(5)	0.0220(5)
O1	3a	0.33333	0.66667	0.66667	0.022(3)
H1	18f	0.404	0.7382	0.66667	0.0296(15)
O2	18f	0.8092(8)	0.8023(8)	0.5435(3)	0.0119(4)
H2	18f	0.7874(15)	0.8040(13)	0.5946(8)	0.0296(15)
O3	18f	0.5295(8)	0.6618(12)	0.5578(3)	0.0119(4)
H3	18f	0.5625(16)	0.668(2)	0.6099(6)	0.0296(15)
O4	18f	0.5091(8)	0.8421(8)	0.4642(3)	0.0119(4)
H4	18f	0.5024(17)	0.8255(16)	0.4076(7)	0.0296(15)

We have used X-ray diffraction to prove the ideal cation order of the Y and Cu, and neutron diffraction to identify and precisely refine the positions of the hydrogen atoms in the structure, since the scattering contrast of hydrogen is sufficiently high in neutron diffraction (scattering length is negative, $b_H = -3.739$ fm, as opposed to +7.75, +7.718, +5.803, and +9.577 fm for Y, Cu, O, and Cl, correspondingly), which allowed for a refinement of the atomic positions of hydrogen in the structure. Using a sample produced with chemicals containing natural hydrogen (and not deuterium, as usually done for a neutron diffraction study) did of course condition a rather high background of incoherent scattering in the pattern, thus a longer acquisition time was needed to achieve sufficient statistics for a reliable refinement. We note that using a third Cl place instead of the proposed O1 and H1 places would lead to the stoichiometry $\text{YCu}_3(\text{OH})_6\text{Cl}_3$ similar to the structure of Ref. [15]. Neutron refinement indicates the absence of the H1 atom, thus only fully occupied

O1, the result was not taken into account due to charge balance.

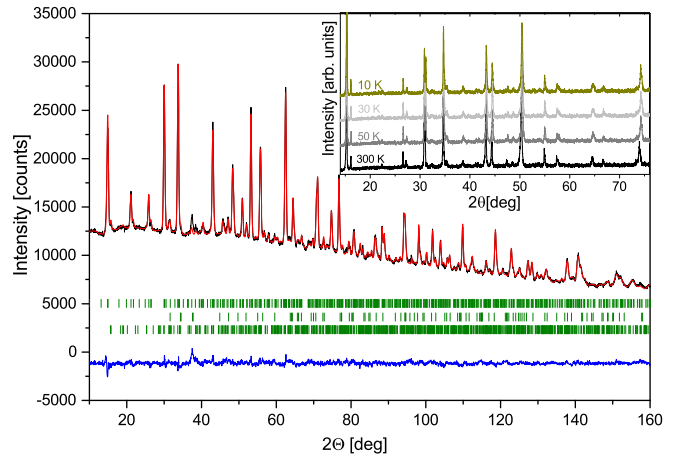


FIG. 2. Rietveld refinement of the crystal structure parameters from neutron powder diffraction data measured at $T = 295$ K. The observed intensity (black), calculated profile (red), and difference curve (blue) are shown of a powder sample. The rows of ticks at the bottom correspond to the calculated diffraction peak positions of the phases (from top to bottom): $\text{Y}_3\text{Cu}_9(\text{OH})_{19}\text{Cl}_8$, CuO 2.5(2) wt%, and $\text{Cu}_2(\text{OH})_3\text{Cl}$ 5.8(2) wt%. Inset: Low-temperature powder X-ray diffraction at different temperatures.

The phase stability at various temperatures was investigated using powder X-ray diffraction (PXRD) data at 10 K - 300 K in 20 K steps. The inset in Fig. 2 reveals that no structural phase transition could be resolved down to 10 K.

The two structure types are further compared in Fig. 3, where we present PXRD data of the two Y-Cu-OH-Cl compounds. For that we have reproduced the synthesis method of Ref. [15]. From Fig. 3 it is obvious, that a discrimination between the two compounds can be easily done using PXRD.

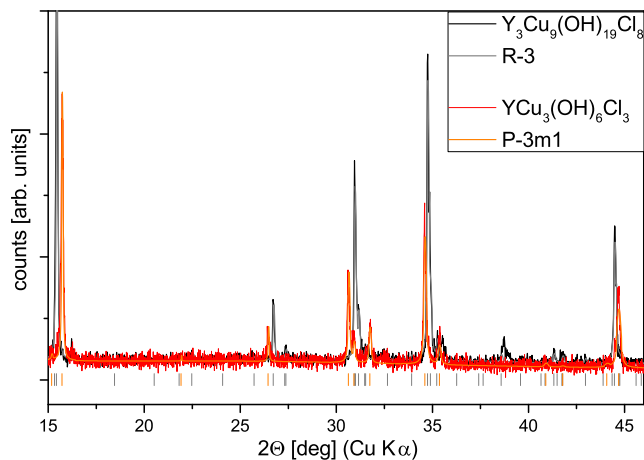


FIG. 3. Powder X-ray diffraction data of the hydrothermally grown $Y_3Cu_9(OH)_{19}Cl_8$ (black) with an underlying refinement of the $R\bar{3}$ structure (grey) compared to the diffraction of a $YCu_3(OH)_6Cl_3$ sample (red) with the $P\bar{3}m1$ structure refinement (orange).

B. Optical measurements

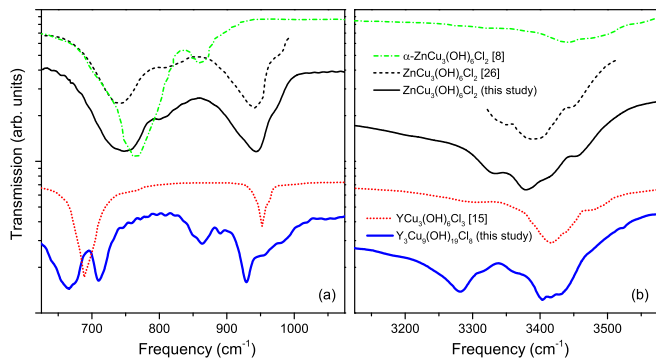


FIG. 4. Powder transmission measurements in the mid-infrared spectral range reveal pronounced differences between the Kagome-lattice compounds $YCu_3(OH)_6Cl_3$ (red dotted line), $Y_3Cu_9(OH)_{19}Cl_8$ (blue), α - $ZnCu_3(OH)_6Cl_2$ (Kapellasite, green) and $ZnCu_3(OH)_6Cl_2$ (Herbertsmithite, black). For the latter compound, our data (full line) match perfectly with literature (dashed line) [26]. Similar as for the two $ZnCu_3(OH)_6Cl_2$ polymorphs, there are striking differences in the optical response between $YCu_3(OH)_6Cl_3$ from Ref. [15] and $Y_3Cu_9(OH)_{19}Cl_8$ which reflects the structural differences like bond lengths and angles. While the vibrational features in the range $700 - 1000 \text{ cm}^{-1}$ are associated with CuO-H deformations (a) and thus give information about the kagome layer, O-H stretching vibrations are observed between 3200 and 3500 cm^{-1} (b) [26, 27].

As these materials are insulators, the electrodynamic response in the mid-infrared range is dominated by phonons. Following the assignment of previous studies, the features around $700 - 1000$ and $3200 - 3500 \text{ cm}^{-1}$ are related to CuO-H deformations in the Kagome layer and O-H stretching vibrations, respectively. In

Fig. 4, we plot the optical transmission spectra for the related Kagome-lattice compounds $YCu_3(OH)_6Cl_3$ (from Ref. [15]), $Y_3Cu_9(OH)_{19}Cl_8$, α - $ZnCu_3(OH)_6Cl_2$ (Kapellasite, Ref. [8]) and $ZnCu_3(OH)_6Cl_2$ (Herbertsmithite, our study and Ref. [26]). There are striking differences between the two $ZnCu_3(OH)_6Cl_2$ polymorphs, such as the absence (or strong softening) of the 940 cm^{-1} mode in Kapellasite, which reflects the structural differences like bond lengths and angles. Similarly, we clearly observe severe discrepancies between $YCu_3(OH)_6Cl_3$ from Ref. [15] and $Y_3Cu_9(OH)_{19}Cl_8$: Comparing the two we find a shift and splitting of the modes around 928 cm^{-1} and 700 cm^{-1} , respectively, as well as additional peaks at 860 cm^{-1} and 3280 cm^{-1} , confirming the structural differences in these compounds, which is consistent with the discussed structure details.

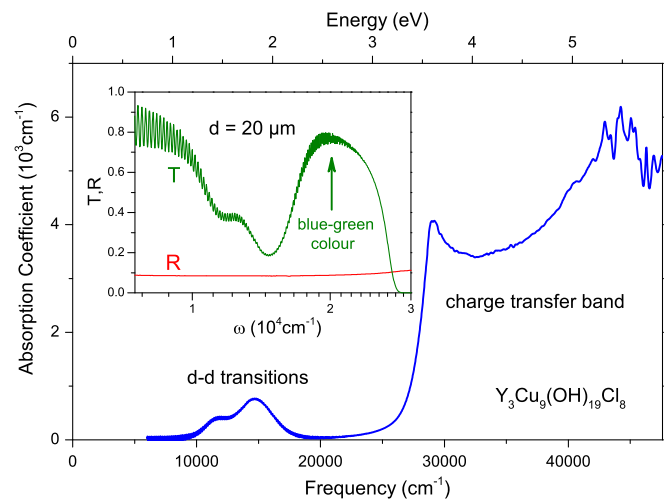


FIG. 5. The VIS-UV absorption spectrum of $Y_3Cu_9(OH)_{19}Cl_8$ reveals the typical features of transition-metal oxides with d-d transitions in the visible range and the charge-transfer band in the UV. Inset: Pronounced Fabry-Perot fringes occur in the transmission data yielding a refractive index of $n \approx 1.7 - 1.8$ in agreement with the optical reflectivity that is basically flat and featureless in the visible range. As a consequence of the absorption in the long-wavelength range, the largest transmission occurs at around $20,000 \text{ cm}^{-1}$ causing the blue-green colour of the crystals.

In addition, we have performed optical transmission experiments on thin single crystals to study the electronic excitations in the visible and ultraviolet spectral ranges. The absorption spectrum shown in Fig. 5 reveals the crystal field splitting of Cu d -orbitals due to Jahn-Teller distortions in the visible and the charge-transfer band with a van-Hove like peak at $29,100 \text{ cm}^{-1}$ (3.6 eV) in the UV. The d-d transitions have maxima at $11,500$ and $14,700 \text{ cm}^{-1}$ which is in the typical range of copper-oxides [28, 29]. The blue-green colour of the crystals stems from the transmission maximum at $20,000 \text{ cm}^{-1}$. From our optical experiments at lower frequencies we found no indication of the Dirac bands [14]. This agrees with the

stoichiometry as the excess charge of the Y^{3+} cations is balanced by Cl^-/OH^- anions and the kagome layer is actually not doped.

C. Magnetic susceptibility and specific heat

In Fig. 6, we present the inverse susceptibility of $Y_3Cu_9(OH)_{19}Cl_8$ measured on a single crystal for two different directions of the magnetic field. In the temperature range 100-300 K, a clear Curie-Weiss behaviour is observed with a large negative Weiss temperature of $\Theta_W = -100$ K for fields perpendicular to the kagome plane indicating a strongly antiferromagnetic mean-exchange field. The effective moment for a magnetic field applied perpendicular to the kagome plane is $\mu_{eff} \approx 2.07 \mu_B/Cu$ resulting in a Landé factor of $g \approx 2.39$, assuming a simple $J = S = 1/2$ coupling system, typical for Cu^{2+} . For fields in the kagome plane, the Curie-Weiss fit yields: $\mu_{eff} \approx 1.89 \mu_B/Cu$, $\Theta_W = -86$ K and $g \approx 2.18$. The leading exchange coupling is most likely within the kagome plane, as the interplane-Cu-Cu distances are much longer compared to the inplane distances. The Weiss temperatures of $Y_3Cu_9(OH)_{19}Cl_8$ are quite similar to the results of W. Sun et al. for magnetic measurements on powders of $YCu_3(OH)_6Cl_3$ with $\Theta_W = -99.2$ K [15] indicating, that the leading exchange couplings in the two Y-Cu-OH-Cl kagome systems are rather similar.

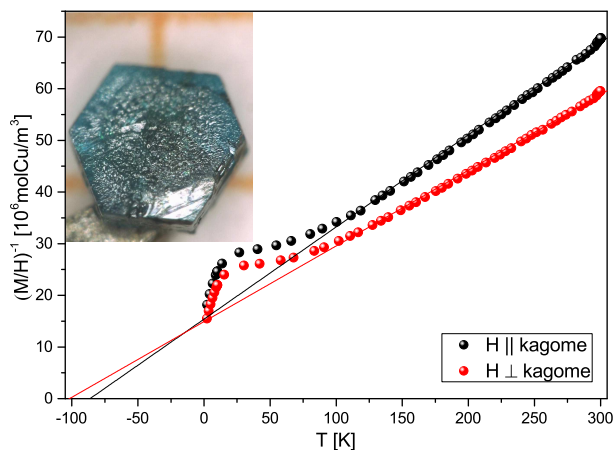


FIG. 6. Inverse magnetization of a $Y_3Cu_9(OH)_{19}Cl_8$ single crystal ($m = 1.34$ mg) in SI units for the two field-directions, parallel and perpendicular to the kagome layers at $H = 1$ T from 300 to 1.8 K. A linear Curie-Weiss fit was done at high temperatures (lines). The image in the inset shows a picture of a $1 \times 1 \times 0.15$ mm³ sized crystal with a mass of 1 mg.

We performed specific-heat measurements on $Y_3Cu_9(OH)_{19}Cl_8$ single crystals in the temperature range from 0.35 to 270 K. While all powder samples contain small amounts of Clinoatacamite only some

crystals have Clinoatacamite twinings on their surface leading to an anomaly at 6.5 K from the magnetic ordering of this impurity phase [6, 9]. The phase stability of $Y_3Cu_9(OH)_{19}Cl_8$ is close to that of Clinoatacamite and always both phases are formed if the hydrothermal growth conditions are applied that are described above. In magnetic measurements, the impurity contribution can even dominate the signal and we have taken great care to select a crystal without this impurity phase. In Fig. 7, the temperature and magnetic-field dependent specific heat of a single crystal without any impurity phase is shown. In zero field (black curve) a maximum is apparent at around 2.2 K. This maximum is slightly shifted to lower temperatures with increasing field approaching ~ 2.0 K at $\mu_0 H = 9$ T, for H parallel to the kagome layer. A small shoulder appears at the low temperature side for fields larger than 3 T. The entropy gain within the maximum in the specific heat at zero field is $S = \int_{0.3}^{4.5} \frac{C_{mol}}{T} dT \approx 0.59 \frac{J}{mol \cdot K} \approx 0.1R \cdot \ln 2$. This shows that the ordered moment of $Y_3Cu_9(OH)_{19}Cl_8$ is strongly reduced and a large portion of the spin degrees of freedom remain fluctuating. We have not subtracted any phononic contribution for the entropy analysis, because at 4 K the estimated contribution of the phonons amounts to only 5%. The phononic contribution was estimated in the range of 8 K to 26 K. The result of a linear fit of C_{mol}/T vs T^2 gives $\gamma_0 = 0.67(2)$ J/(molK²) and $\beta_0 = 3.38(6)$ mJ/(molK⁴). This yields a Debye temperature of $\theta_D \approx 318$ K. In addition, we do not observe any phase transition in the temperature range from 8 to 270 K, in agreement with the magnetic measurements and the temperature dependent PXRd. The low ordering temperature together with the large Weiss-temperature gives a frustration parameter $\Theta_W/T_N \approx 50$, proving that $Y_3Cu_9(OH)_{19}Cl_8$ is still a strongly frustrated material. Above T_N , the specific heat of $Y_3Cu_9(OH)_{19}Cl_8$ follows a linear in T-dependence up to 8 K most likely due to the enhanced spin fluctuations.

We have also measured the specific heat of a powder sample of $YCu_3(OH)_6Cl_3$ (orange curves in Fig. 7), which clearly shows the absence of magnetic order down to 0.4 K which is in agreement with the proposal of a spin-liquid ground state by W. Sun et al. [15]. Our low-temperature measurements enhance the lower boundary of the frustration parameter of $YCu_3(OH)_6Cl_3$ to $\Theta_W/T_N > 250$ and clearly proves the different magnetic ground states of the two Y-Cu-OH-Cl compounds. The same linear fit procedure was done for a specific heat measurement of $YCu_3(OH)_6Cl_3$ giving $\gamma_0 = 0.27(1)$ J/(molK²), $\beta_0 = 1.22(3)$ mJ/(molK⁴) and $\theta_D \approx 312$ K, revealing the structural similarity of these systems. Again, no phase transitions were observed up to 250 K.

The magnetic transition at T_N of $Y_3Cu_9(OH)_{19}Cl_8$ can

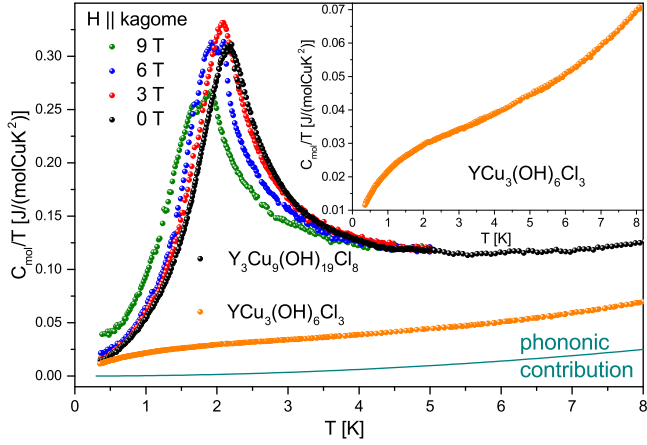


FIG. 7. Specific-heat divided by temperature at various magnetic fields of an impurity-free $Y_3Cu_9(OH)_{19}Cl_8$ single crystal and an $YCu_3(OH)_6Cl_3$ powder sample with the $P\bar{3}m1$ structure. In the inset, the zero field curve of $YCu_3(OH)_6Cl_3$ is enlarged and it is apparent, that no long-range magnetic order occurs in the investigated temperature range.

also be determined by magnetic measurements in phase pure crystals, which show a broad maximum at 2.5 K (see Fig. 8). This broad transition is in contrast to the well-defined anomaly in the specific-heat measurements and might be due to a large magnetic background because of enhanced spin-fluctuations of that material. The magnetization is larger for magnetic fields applied perpendicular to the kagome planes, but the overall magnetic anisotropy is weak. The $M(H)$ curve perpendicular to the field (inset of Fig. 8) shows a nearly linear increase, while the parallel one has a small kink above 2 T. This might be related to the field induced shoulder observed in the specific heat data. Both $M(H)$ curves show no saturation up to 9 T. In comparison with Herbertsmithite, the magnetic anisotropy in $Y_3Cu_9(OH)_{19}Cl_8$ is stronger but also favors the c -direction as the easy magnetic axis [30].

IV. CONCLUSION

In conclusion, $Y_3Cu_9(OH)_{19}Cl_8$ is a stoichiometric quantum spin system with well-separated kagome layers of localized Cu^{2+} spins. Detailed structural refinements of hydrothermally prepared single crystals revealed a crystal structure with two different copper positions, leading to slightly anisotropic kagome layers. These structural modifications were corroborated by optical absorption experiments which, in addition, confirmed the chemical composition as the studied material shows insulating behaviour with no indications of electron doping and the proposed Dirac bands.

The partial release of magnetic frustration within the

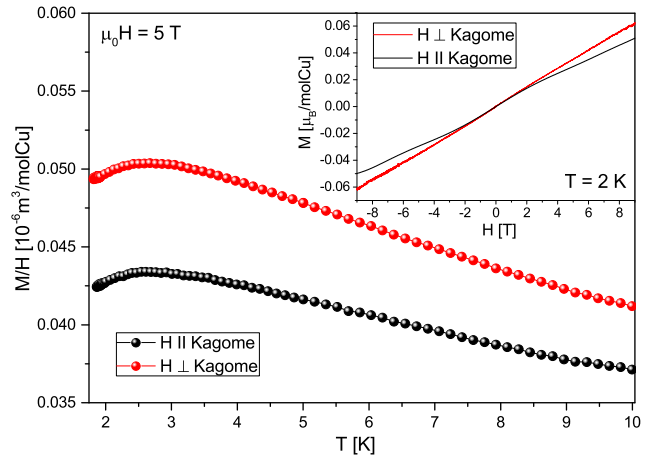


FIG. 8. Molar susceptibility of a $Y_3Cu_9(OH)_{19}Cl_8$ single crystal measured at 5 T from $T = 10$ K to 1.8 K. Inset: the magnetization versus field curve measured at 2 K along and perpendicular to the kagome layers.

kagome layers compared to $YCu_3(OH)_6Cl_3$ is also reflected in the magnetic properties, because we observe weak but clear magnetic order at $T_N = 2.2$ K in magnetization and specific-heat measurements on single crystals of $Y_3Cu_9(OH)_{19}Cl_8$. However, the frustration effects are still very pronounced with a frustration parameter of $\frac{\theta_W}{T_N} \sim 50$.

Low-temperature specific-heat measurements on a powder sample of $YCu_3(OH)_6Cl_3$ revealed the absence of magnetic order down to 0.4 K, leading to a frustration parameter $\Theta_W/T_N > 250$. Therefore, the two Y-Cu-OH-Cl compounds present an unique setting to investigate the change from a spin-liquid state to a strongly frustrated AFM ordered state, by slightly releasing the frustration in a kagome lattice via structural modification. Unlike for substitution series, as e.g. $Zn_xCu_{4-x}(OH)_6Cl_2$, where we always encounter crystallographic disorder, the magnetic properties of the two stoichiometric compounds with fully occupied kagome sites might be much more reliable with ab-initio calculations. Additionally, these two stoichiometric kagome systems might open the way for a systematic understanding of magnetic frustration in kagome materials, which would require further more microscopic measurements of the spin-fluctuation spectrum in these two systems.

The authors gratefully acknowledge support by the Deutsche Forschungsgemeinschaft through grant SFB/TR 49. We thank Michael Seitz for the help with the LA-ICP-MS measurements. This work is based on experiments performed at the Swiss spallation neutron source SINQ, Paul Scherrer Institute, Villigen, Switzerland.

-
- [1] L. Balents, Nature **464**, 199 (2010)
- [2] M. P. Shores, E. A. Nytko, B. M. Barlett, and D. G. Nocera: J. Am. Chem. Soc. **127**, 13462 (2005)
- [3] P. Mendels et al., Phys. Rev. Lett. **98**, 077204 (2007)
- [4] T-H. Han, J. S. Helton, S. Chu, D. G. Nocera, J. A. Rodriguez-Rivera, C. Broholm and Y. S. Lee, Nature **492**, 406–410 (2012)
- [5] J. S. Helton et al., Phys. Rev. Lett. **98**, 107204 (2007)
- [6] M. R. Norman, Rev. Mod. Phys. **88**, 041002 (2016)
- [7] D. E. Freedman et al., J. Am. Chem. Soc. **132**, 16185–16190 9 16185 (2010)
- [8] W. Krause et al., Mineral. Mag. 70(3), 329 (2006)
- [9] S. Chu, P. Müller, D. G. Nocera, and Y. S. Lee, Applied Phys. Lett. **98**, 092508 (2011)
- [10] H. Ishikawa, J.-ichi Yamaura, Y. Okamoto, H. Yoshida, G. J. Nilsena and Z. Hiroia, Acta Cryst. **C68**, i41 (2012)
- [11] D. Boldrin, K. Knight and A. S. Wills, J. Mater. Chem. C **4**, 10315 (2016)
- [12] D. A. Prishchenko, A. A. Tsirlin, V. Tsurkan, A. Loidl, A. Jesche, V. G. Mazurenko, arXiv:1611.03317 (2016)
- [13] W. Sun, Y. Huang, Y. Pan, J. Mi, Phys. Chem. Min. **43**:127–136 (2016)
- [14] I. I. Mazin, H. O. Jeschke, F. Lechermann, H. Lee, M. Fink, R. Thomale, and R. Valentí, Nat. Comm. **5**, 4261 (2014)
- [15] W. Sun, Y. Huang, S. Nokhrin, Y. Pan and J. Mi, J. Mater. Chem. C **4**, 8772-8777 (2016)
- [16] R. H. Colman, C. Ritter, and A. S. Wills, Chem. Mater. **20**, 22 (2008)
- [17] R. H. Colman, A. Sinclair, and A. S. Wills, Chem. Mater. **23**, 1811–1817 (2011)
- [18] T. M. McQueen, T.H.Han, D.E.Freedman, P.W.Stephens, Y.S.Lee, D.G.Nocera, J. Solid State Chem. **184**, 3319–3323 (2011)
- [19] G. Meyer, *The Ammonium Chloride Route to Anhydrous Rare Earth Chlorides-The Example of YCl₃*, Inorganic Syntheses **25**, 146–150 (1989)
- [20] P. Melnikov, V. A. Nascimento, L. Z. Z: Consolo and A. F. Silva, J. Therm. Anal. Calorim. **111**, 115-119 (2013)
- [21] Stoe and Cie GmbH, X-AREA. Diffractometer control program system (2002)
- [22] G. M. Sheldrick, Acta Cryst. A **64**, 112-122 (2008)
- [23] P. Fischer et al., Physica B **276-278**, 146 (2000)
- [24] J. Rodriguez-Carvajal, Physica B. **192**, 55 (1993)
- [25] D. Guterding, H. O. Jeschke & R. Valentí, Sc. Rep. **6**, 25988 (2016)
- [26] R. S. W. Braithwaite, K. Mereiter, W. H. Paar and A. M. Clark, Mineral. Mag. **68**(3), 527 (2004)
- [27] A. B. Sushkov G. S. Jenkins, T. H. Han, Y. S. Lee, H. D. Drew, J. Phys.: Condens. Matter **29**, 095802 (2017)
- [28] S. J. Hwu et al., J. Am. Chem. Soc. **124**, 12404 (2002)
- [29] M. Sala et al., New J. of Phys. **13**, 043026 (2011)
- [30] T. H. Han, J. S. Helton, S. Chu, A. Prodi, D. K. Singh, Mazzoli, P. Müller, D. G. Nocera, and Y. S. Lee, Phys. Rev. B **83**, 100402(R) (2011)